Available online at http://scik.org
J. Math. Comput. Sci. 5 (2015), No. 1, 99-122
ISSN: 1927-5307

NUMERICAL STUDY OF COUPLED FLUID FLOW WITH HEAT AND MASS TRANSFER USING FINITE VOLUME DISCRETIZATION

V. AMBETHKAR

Department of Mathematics, Faculty of Mathematical Sciences, University of Delhi, Delhi 110007, India

Abstract. This paper presents a finite volume discretization for the numerical solution of the semi-linear partial differential equations together with suitable initial and the boundary conditions that describe the fluid flow coupled with heat and mass transfer. Heat and mass transfer has been predicted with the aid of a staggered grid of finite volume discretization. The numerical results for the flow variables velocity, pressure, temperature and concentration have been computed by employing the SIMPLE algorithm. The numerical results show that the pressure of the fluid at different nodes increasing uniformly either by keeping step size in one direction fixed and in other direction varied. The variation of the concentration considered in z-direction vis-á-vis grid nodes in x and y-direction has been plotted and examined using 3-D graphs. It is found that the heat and mass transfer for fluids like mercury, air, and water increasing towards left side of the domain of the computation. Based on the numerical results, it has been found that the mass transfer increases steadily and then decreases while moving in grid nodes along y-direction for a fixed node along x-direction.

Keywords: finite volume discretization, mass transfer, heat transfer, SIMPLE algorithm, Reynolds number, Schmidt number, Prandtl number, staggered grid, u-velocity, v-velocity, pressure, temperature, concentration.

2010 AMS Subject Classification: 65M08, 65N08, 74S10, 76M12, 80A20

1. Introduction

Received July 23, 2014

Coupled fluid flow with heat and mass transfer plays an important role in various equipment and process. Heat and mass transfer from small cavities has many engineering and much other large number of practical applications. For instance, metallization processes for electronic packaging or interconnects involves electrochemical deposition into very small cavities which have been created by technologies such as photolithography. It has other applications including in heat exchangers, turbine systems, internal combustion engines, cooling systems for electric motors, generators, transforms, in chemical plants, in ammonia refrigeration systems, air-conditioning applications, evaporation of petrol in internal combustion engines, neutron diffusion in nuclear reactors, etc. The finite volume method is a method for representing and evaluating partial differential equations in the form of algebraic equations. Similar to the finite difference method or finite element method, values are calculated at discrete places on a meshed geometry. To perform a numerical simulation, the flow geometry has to be represented by a computational mesh consisting of a large number of computational cells denoting the volume in the present method of finite volume.

Numerical calculation of time-dependent viscous incompressible flow of fluid with free surface has been investigated by Harlow and Welch [1]. Heat and mass transfer on moving continuous flat plate with suction or injection has been studied by Erickson *et al*. [2]. Chorin [3] presented a numerical solution of Navier-Stokes equations. Patankar and Spalding [4] described a calculation procedure for heat, mass and momentum transfer in three-dimensional parabolic flows. Gupta and Gupta [5] studied heat and mass transfer on a stretching sheet with suction or blowing. Ghia *et al.* [7], Mansour and Hamed [13] and Bruneau and Jouron [14] had used a multigrid method on non-staggered grid to present high-resolution for the Navier-Stokes equations of an incompressible viscous flow. Chen *et al.* [10] investigated effect of external laminar channel flow on mass transfer in a cavity. Three-dimensional unsteady flow with heat and mass transfer over a continuous stretching surface has been examined by Lakshmisha *et al.* [11].

Effect of fluid flow on convective transport in small cavities, accurate solution to the square thermally driven cavity at high Rayleigh number, convective mass transport from rectangular cavities, effect of the aspect ratio on the transient mass/ heat transfer in an open cavity and effect of an unsteady external flow on mass transfer to cavities have been investigated by Alkire *et al.*

[15], Quere [17], Occhialini and Higdon [18], Chen [21] and Shehata *et al.* [32]. Demirdzic and Peric [16]; Lilek and Peric [19] had presented finite volume method for prediction of fluid flow in arbitrarily shaped domains with moving boundaries especially of fourth order method with collocated variable arrangement. The method uses collocated variable arrangement and the SIMPLE kind of velocity-pressure coupling. Influence of a magnetic field on heat and mass transfer by natural convection from vertical surface in porous media considering Soret and Dufur effects proposed by Postelnicu [24]. Numerical simulations of the 2-D lid-driven cavity flow were performed for a wide range of Reynolds numbers by Bruneau and Saad [26]. Young *et al.* [27] proposed a numerical scheme based on the method of fundamental solutions (MFS) for the solution of 2-D and 3-D Stokes problems. The development of a compact fourth-order finite volume method for solutions of the Navier-Stokes equations on staggered grids was presented by Hokpunna and Manhart [30]. A higher-order divergence-free interpolation for convective velocities was developed which ensures a perfect conservation of mass and momentum on momentum control volumes.

Though there have been many investigations on heat transfer together with fluid flow which include as [8,15,17] and [26], the problem of coupled fluid flow with heat and mass transfer using finite volume discretization has not being investigated widely by the researchers. Moreover, the case of incompressible 2-D or 3-D viscous flow in the literature has been seen in [8,11,19,26] wherein pressure mostly used to be eliminated. Consequently, the governing equations of those problems reduce to much simpler form and had been solved easily. Nowhere in the literature, a cumbersome situation as in the present problem prevailed which neither has been attempted nor examined. This idea has neither been extended nor previously considered in the literature for a suitable problem like the present one. We therefore have been motivated by the present investigation with a view to provide a solution to the above difficulty used to or being faced by the researchers during the past perhaps until now. Hence, in this paper, pressure in momentum equations has been retained. Consequently, the staggered grid approach is inevitable and has been implemented. The well-known SIMPLE algorithm is employed for velocity, pressure, temperature and concentration coupling.

Accordingly, our aim in the present work is to numerically investigate using a finite volume method, the solution of the semi-linear partial differential equations together with suitable initial and boundary conditions that describe the fluid flow coupled with heat and mass transfer past a rectangular domain with slip boundary conditions. An outline of this paper is as follows: In Section 2, we introduce the governing equations, initial and boundary conditions under mathematical formulation. The finite volume disscretization, staggered grid, discretization of momentum, energy, mass transport equations has been detailed under Section 3. The numerical computations of the unknown flow variables u, v, p, T, C have been given under Section 4. Results and discussions have been given under Section 5 and in the final section main conclusions of this study have been summarized.

2. Mathematical formulation

2.1. Governing equations

The governing equations for coupled steady fluid flow with heat and mass transfer past a rectangular domain with slip boundary conditions are given below. The governing equations (1)-(5) subject to the initial and boundary conditions given by Eqs. (6) and (7) are solved using finite volume discretization. Taking usual Boussniesq approximations into account, the governing equations of the problem in dimensionless form become

Continuity equation

$$\frac{\partial u}{\partial x}+\frac{\partial v}{\partial y}=0, \tag{1}$$

x-momentum equation

$$u\frac{\partial u}{\partial x}+v\frac{\partial u}{\partial y}=-\frac{\partial p}{\partial x}+\left(\frac{1}{\mathrm{Re}}\right)\left(\frac{\partial^2 u}{\partial x^2}+\frac{\partial^2 u}{\partial y^2}\right), \tag{2}$$

y-momentum equation

$$u\frac{\partial v}{\partial x}+v\frac{\partial v}{\partial y}=-\frac{\partial p}{\partial y}+\left(\frac{1}{\mathrm{Re}}\right)\left(\frac{\partial^2 v}{\partial x^2}+\frac{\partial^2 v}{\partial y^2}\right), \tag{3}$$

Energy equation

$$u\frac{\partial T}{\partial x}+v\frac{\partial T}{\partial y}=\frac{1}{\mathrm{Pr}}\left(\frac{\partial^2 T}{\partial x^2}+\frac{\partial^2 T}{\partial y^2}\right), \tag{4}$$

Mass transfer equation

$$u\frac{\partial C}{\partial x}+v\frac{\partial C}{\partial y}=\frac{1}{\mathrm{Sc}}\left(\frac{\partial^2 C}{\partial x^2}+\frac{\partial^2 C}{\partial y^2}\right). \tag{5}$$

2.2. Initial and boundary conditions of the problem

The initial and boundary conditions of the above governing equations (1)-(5) are given as

$$\text{for } t=0,\ u(x,y,0)=0,\ v(x,y,0)=0,\ T(x,y,0)=0,\ C(x,y,0)=0, \tag{6}$$

$$\text{for } t>0,$$

$$\text{on boundaries AB and CD}: u=0.0,\ v=0.5,\ T=0.5,\ C=0.5.$$

$$\text{on boundaries BC and AD}: u=1.0,\ v=0.0,\ T=1.0,\ C=1.0. \tag{7}$$

at all four corner points velocities (u,v), temperature (T) and concentration (C) vanishes. It may be noted here that, regarding specifying the boundary conditions for pressure, the convention followed is either the pressure at the boundary is given or the velocity component normal to the boundary is specified.

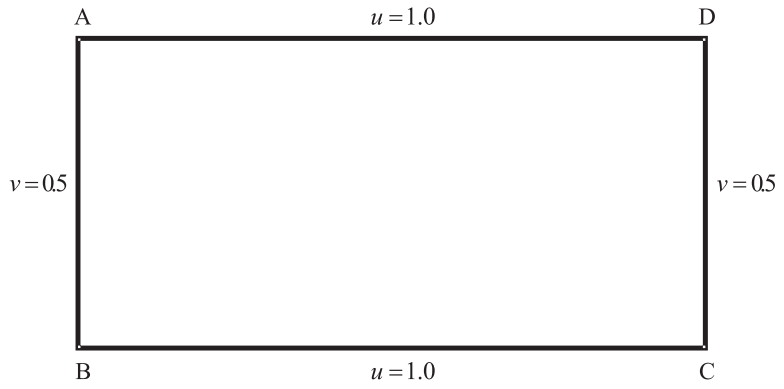

FIGURE 1. Rectangular cavity

3. Finite volume discretization

3.1. The Staggered grid

The finite volume discretization (FVD) has been used for solving numerically the discretized equations (1) to (5) to obtain solutions of u, v, p, T and C of the present problem based on a uniform staggered grid system. A staggered grid [18, pp. 195–200] as shown in Fig. 2 below, contains the scalar variables, including pressure, temperature and concentration are stored at the nodes marked ($\bullet$). The velocities are defined at the (scalar) cell faces in between the nodes and are indicated by arrows. Horizontal ($\rightarrow$) arrows indicate the locations for u-velocities and the vertical ($\uparrow$) ones denote those for v-velocity. In addition to the E, W, N, S notation, the u-velocities are stored at scalar cell faces e and w and the v-velocities at cell faces n and s.

3.2. Discretization of momentum equations

In Fig. 2, the unbroken grid lines are numbered by means of capital letters. In the x-direction the numbering is $\ldots, I-1, I, I+1, \ldots$ etc, and in the y-direction the numbering is $\ldots, J-1, J, J+1, \ldots$ etc. The dashed lines that construct the cell faces are denoted by lower case letters $\ldots, i-1, i, i+1, \ldots$ and $\ldots, j-1, j, j+1, \ldots$ in the x-and y-directions respectively. A subscript system based on this numbering allows us to define the locations of grid nodes and cell faces with precision.

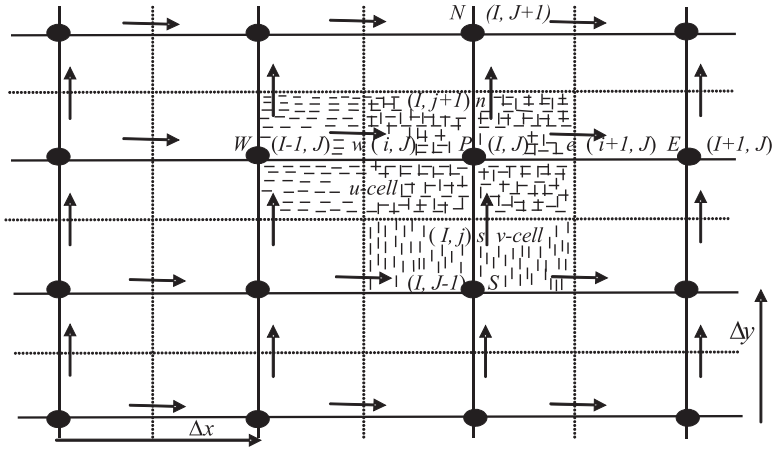

FIGURE 2. Staggered grid

The discretized form of u-momentum equation for the velocity at the location (i,J) has the following form:

$$a_{i,J}u_{i,J} = \sum a_{nb}u_{nb} + (p_{I-1,J} - p_{I,J})A_{i,J}\,. \tag{8}$$

Where $A_{i,J}$ is the (east or west) cell face area of the u-control volume. In the new numbering system the E, W, N and S neighbors involved in the summation $\sum a_{nb}u_{nb}$ are $(i+1,J)$, $(i-1,J)$, $(i,J+1)$, and $(i,J-1)$. Their locations and the prevailing velocities are shown in the Fig. 3. The values of coefficients in Eq. (8) corresponding to the hybrid differencing scheme are as follows:

$$\begin{cases} a_W = \max\left[F_w, \left(D_w + \dfrac{F_w}{2}\right), 0\right], \quad a_E = \max\left[-F_e, \left(D_e - \dfrac{F_e}{2}\right), 0\right], \\ a_S = \max\left[F_s, \left(D_s + \dfrac{F_s}{2}\right), 0\right], \quad a_N = \max\left[-F_n, \left(D_n - \dfrac{F_n}{2}\right), 0\right], \\ a_P = a_W + a_E + a_S + a_N + (F_e - F_w) + (F_n - F_s). \end{cases} \tag{9}$$

The coefficients contain combinations of the convective flux per unit mass F and the diffusive conductance D at u-control volume cell faces. Applying the new notation system we give the values of F and D for each of the faces e, w, n and s of the u-control volume:

$$\begin{cases} F_w = (u)_w = \dfrac{1}{2}(u_{i,J} + u_{i-1,J}), \quad F_e = (u)_e = \dfrac{1}{2}(u_{i+1,J} + u_{i,J}), \\ F_s = (v)_s = \dfrac{1}{2}(v_{I,j} + v_{I-1,j}), \quad F_n = (v)_n = \dfrac{1}{2}(v_{I,j+1} + v_{I-1,j+1}), \\ D_w = \dfrac{1}{\mathrm{Re}(x_i - x_{i-1})}, \quad D_e = \dfrac{1}{\mathrm{Re}(x_{i+1} - x_i)}, \\ D_s = \dfrac{1}{\mathrm{Re}(y_J - y_{J-1})}, \quad D_n = \dfrac{1}{\mathrm{Re}(y_{J+1} - y_J)}. \end{cases} \tag{10}$$

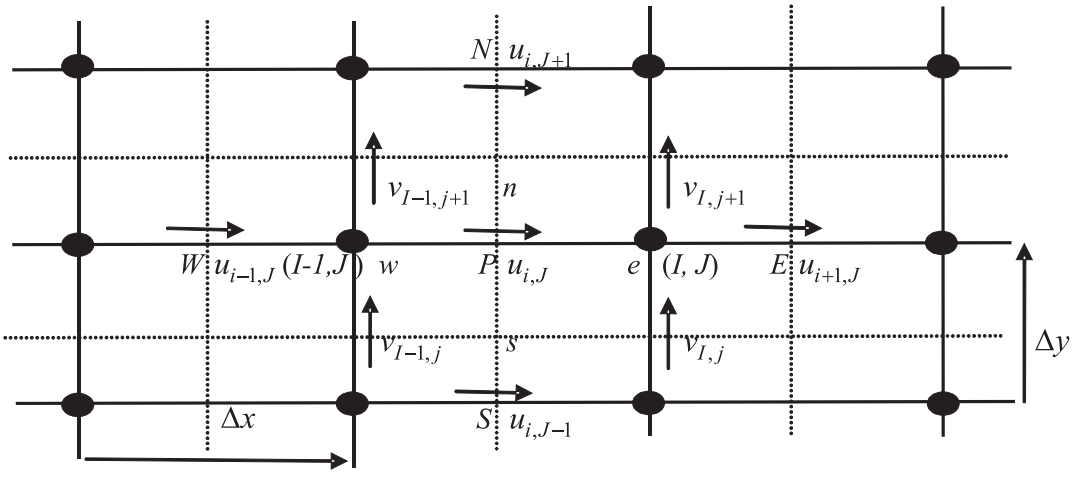

FIGURE 3. A u-control volume and its neighboring velocity components

By analogy the discretized form of v-momentum equation becomes as:

$$a_{I,j}v_{I,j} = \sum a_{nb}v_{nb} + (p_{I,J-1} - p_{I,J})A_{I,j}\,. \tag{11}$$

The neighbors involved in the summation $\sum a_{nb}v_{nb}$ and prevailing velocities are as shown in the Fig. 4.

The discretized pressure correction equation due to scalar control volume as shown in Fig. 5 has the following form:

$$a_{I,J}p'_{I,J} = a_{I+1,J}p'_{I+1,J} + a_{I-1,J}p'_{I-1,J} + a_{I,J+1}p'_{I,J+1} + a_{I,J-1}p'_{I,J-1} + b'_{I,J}\,. \tag{12}$$

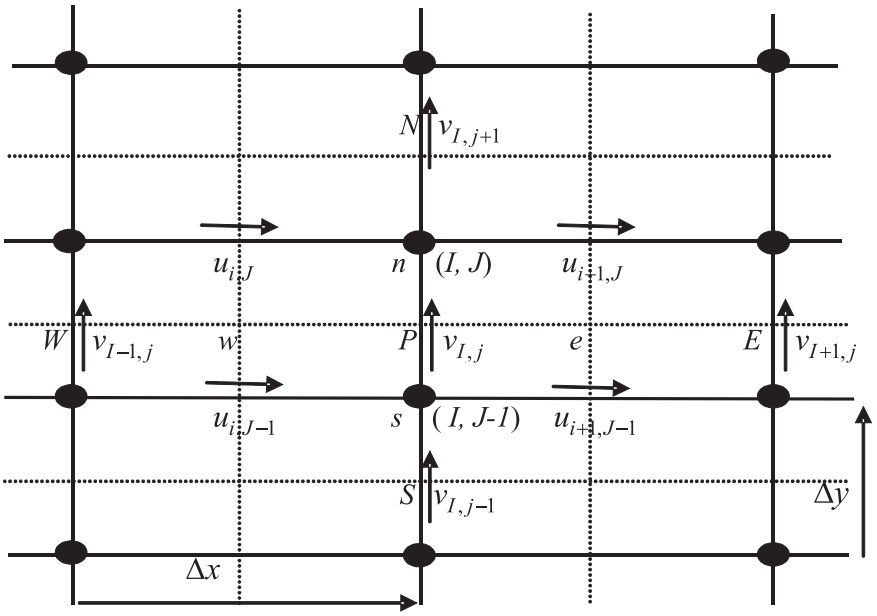

FIGURE 4. A v-control volume and its neighboring velocity components

Where

$$\begin{cases} a_{I,J} = a_{I+1,J} + a_{I-1,J} + a_{I,J+1} + a_{I,J-1}, \;\; a_{I+1,J} = (dA)_{i+1,J}, \\ a_{I-1,J} = (dA)_{i,J}, \;\; a_{I,J+1} = (dA)_{i,J+1}, \;\; a_{I,J-1} = (dA)_{i,J} \end{cases} \tag{13}$$

$$d_{i,J} = \frac{A_{i,J}}{a_{i,J}}, \;\; d_{I,j} = \frac{A_{I,j}}{a_{I,j}}, \tag{14}$$

$$b'_{I,J} = (u^*A)_{i,J} - (u^*A)_{i+1,J} + (v^*A)_{I,j} - (v^*A)_{I,J+1}. \tag{15}$$

The discretized equations for temperature and the concentration have the following form:

$$a_P T_P = a_W T_W + a_E T_E + a_S T_S + a_N T_N, \tag{16}$$

and

$$a_P C_P = a_W C_W + a_E C_E + a_S C_S + a_N C_N \tag{17}$$

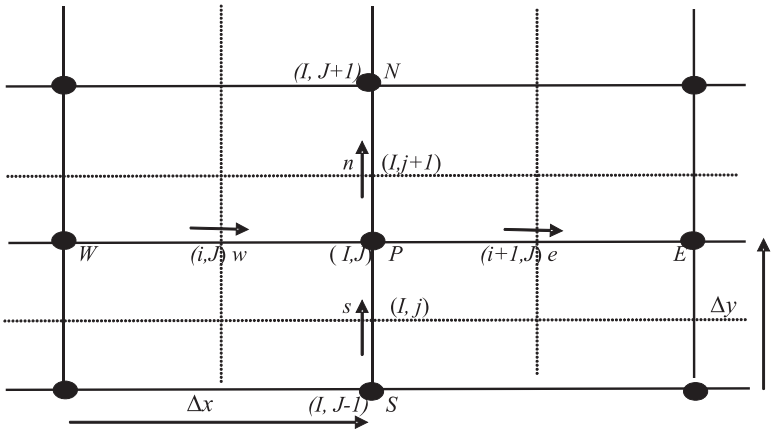

FIGURE 5. Scalar control volume (continuity equation)

Where:

$$\begin{cases} a_W = \max\left[F_w, \left(D_w + \dfrac{F_w}{2}\right), 0\right], & a_E = \max\left[-F_e, \left(D_e - \dfrac{F_e}{2}\right), 0\right], \\ a_S = \max\left[F_s, \left(D_s + \dfrac{F_s}{2}\right), 0\right], & a_N = \max\left[-F_n, \left(D_n - \dfrac{F_n}{2}\right), 0\right], \end{cases} \tag{18}$$

$$a_P = a_W + a_E + a_S + a_N + (F_e - F_w) + (F_n - F_s), \tag{19}$$

$$\begin{cases} F_w = (u)_w = u_{i,J}, & F_e = (u)_e = u_{i+1,J}, \\ F_s = (v)_s = v_{I,j}, & F_n = (v)_n = v_{I,j+1}, \\ D_w = \dfrac{1}{\mathrm{Re}(x_I - x_{I-1})}, & D_e = \dfrac{1}{\mathrm{Re}(x_{I+1} - x_I)}, \\ D_s = \dfrac{1}{\mathrm{Re}(y_J - y_{J-1})}, & D_n = \dfrac{1}{\mathrm{Re}(y_{J+1} - y_J)}. \end{cases} \tag{20}$$

4. Numerical computations

The numerical computations of the five unknown flow variables u, v, p, T, C have been obtained from their five discretized equations (8), (11), (12), (16) and (17) at each time level by the SIMPLE algorithm which in turn executed with the aid of a computer program developed and run on C-compiler. The input data for the relevant parameters in the governing equations like Re, Pr and Sc have been properly chosen by considering physical significance of the present problem.

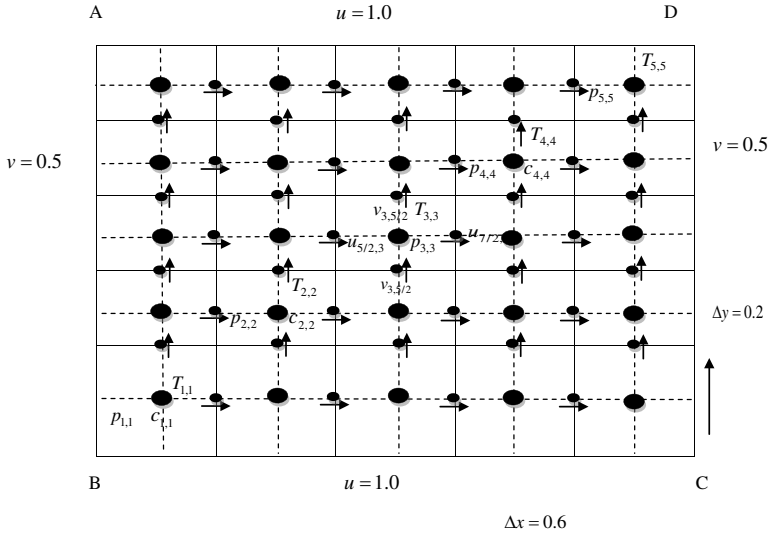

FIGURE 6. Computational staggered grid

The acronym SIMPLE stands for Semi-Implicit Method for Pressure-Linked Equations. The algorithm was originally put forward by Patankar and Spalding [4] and essentially a guess-and-correct procedure for the calculation of pressure on a staggered grid arrangement introduced above. The algorithm gives a method of calculating pressure, velocities, temperature and concentration. The method is iterative, and when other scalars are coupled to the momentum equations the calculation needs to be done sequentially. The sequence of operations which employ the SIMPLE algorithm is given below.

4.1. The SIMPLE algorithm

The steps in the SIMPLE algorithm for solving coupled fluid flow, heat and mass transfer can be summarized as follows:

1. Start with an initial guess for the velocities u^*, v^*, pressure fields p^*, temperature T^* and concentration C^*.

2. Calculate the coefficients in the momentum equation, solve discretized momentum equations.

3. Calculate the coefficients of the pressure equation, solve pressure correction equation.

4. Correct pressure and velocities:

$$p_{I,J} = p^*_{I,J} + p'_{I,J}, \;\; u_{i,J} = u^*_{i,J} + d_{i,J}(p'_{I-1,J} - p'_{I,J}),$$

$$v_{I,j} = v^*_{I,j} + d_{I,j}(p'_{I,J-1} - p'_{I,J}).$$

5. Solve the discretized equations for temperature and concentration.

6. Replace the previous intermediate values of pressure and velocity $(p^*, u^*, v^*, T^*, C^*)$ until the corrected values (p, u, v, T, C), return to **2** and repeat the whole process until the solution converges.

5. Results and discussion

In order to get clear insight into the present problem, the numerical computations of u-velocity, v-velocity, pressure, temperature and concentration for Reynolds number $\mathrm{Re} = 1000$, different Prandtl number $\mathrm{Pr} = 0.04, 0.733, 6.75$ and the Schmidt numbers $\mathrm{Sc} = 0.22, 0.60, 0.75$ by the method described under section 3 has been done using an algorithm described under Section 4.1. The Prandtl and Schmidt numbers which have been chosen as $\mathrm{Pr} = 0.04, 0.733, 6.75$ corresponds to mercury, air and water and $\mathrm{Sc} = 0.22, 0.60, 0.75$ to hydrogen, watervapour and oxygen respectively by considering the significance of the problem under discussion. The behavior of the flow profiles u-velocity, v-velocity, pressure, temperature and concentration has been described with the help of the numerical solutions shown in Tables 1 to 4.

The numerical results of u-velocity for $\mathrm{Re} = 1000$ at different nodes have been shown in Table 1. The behavior of u-velocity has been illustrated in Fig. 7. It can be seen that for fixed values of y, u-velocity decreases initially and then keeps on increasing uniformly as we move from left boundary to the right boundary. Similarly the numerical results of v-velocity for $\mathrm{Re} = 1000$ at different nodes have been shown in Table 2. The behavior of v-velocity has

been depicted in Fig. 8. It can be seen that for fixed value of x, v-velocity increases at external nodes and has an oscillatory behavior at internal nodes as we move from bottom boundary to top boundary.

TABLE 1. Numerical solutions of u-velocity for $\mathrm{Re} = 1000$.

(x,y)	u-velocity
$(0.6,0.1)$	0.00263
$(1.2,0.1)$	0.00383
$(1.8,0.1)$	0.00477
$(2.4,0.1)$	0.00529
$(0.6,0.3)$	-0.00220
$(1.2,0.3)$	-0.00326
$(1.8,0.3)$	-0.00348
$(2.4,0.3)$	-0.00356
$(0.6,0.5)$	-0.00228
$(1.2,0.5)$	-0.00338
$(1.8,0.5)$	-0.00382
$(2.4,0.5)$	-0.00409
$(0.6,0.7)$	-0.00261
$(1.2,0.7)$	-0.00344
$(1.8,0.7)$	-0.00423
$(2.4,0.7)$	-0.00569
$(0.6,0.9)$	0.00331
$(1.2,0.9)$	0.00344
$(1.8,0.9)$	0.00381
$(2.4,0.9)$	0.00392

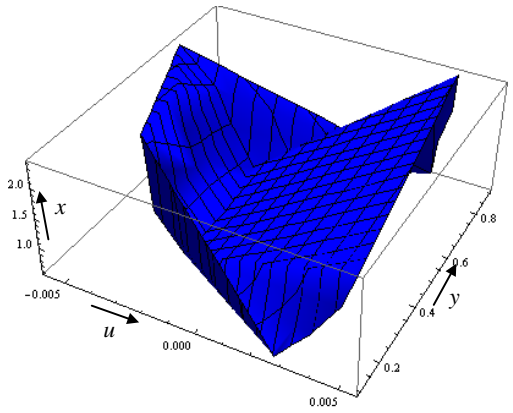

FIGURE 7. u-velocity for $(\mathrm{Re} = 1000)$.

The numerical solutions for the pressure for given values of x and y which varies from 0.0 to 3.0 and 0.0 to 1.0 respectively have been computed and given in Table 3. The behavior of the

pressure of the fluid at different nodes has been illustrated in Fig. 9. It has been observed that either keeping x-fixed or y-varies or keeping y-fixed and the pressure increases uniformly.

TABLE 2. Numerical solutions of v-velocity for $\mathrm{Re} = 1000$.

(x,y)	v-velocity
$(0.3,0.2)$	-0.00162
$(0.3,0.4)$	-0.00052
$(0.3,0.6)$	0.00063
$(0.3,0.8)$	0.00122
$(0.9,0.2)$	-0.00038
$(0.9,0.4)$	-0.00019
$(0.9,0.6)$	0.00078
$(0.9,0.8)$	-0.00066
$(1.5,0.2)$	-0.00056
$(1.5,0.4)$	0.00138
$(1.5,0.6)$	0.00068
$(1.5,0.8)$	-0.00057
$(2.1,0.2)$	-0.00066
$(2.1,0.4)$	0.00079
$(2.1,0.6)$	-0.00082
$(2.1,0.8)$	-0.00078
$(2.7,0.2)$	0.00017
$(2.7,0.4)$	0.00078
$(2.7,0.6)$	-0.00012
$(2.7,0.8)$	-0.00133

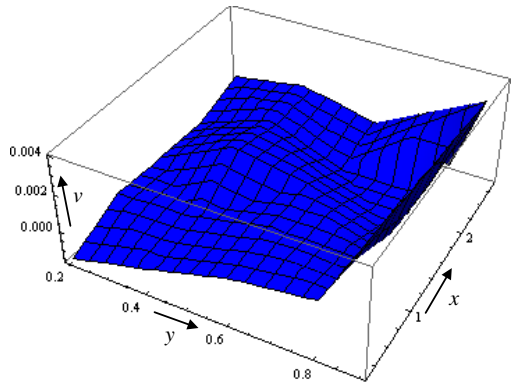

FIGURE 8. v-velocity for $(\mathrm{Re} = 1000)$.

The numerical solutions of temperature for fluid flow for $\mathrm{Re} = 1000$ and for different Prandtl numbers $\mathrm{Pr} = 0.04, 0.733$ and 6.75 have been shown in Table 4. It has been depicted from Table 4 that temperature for fluid at particular value of y increases along x-axis. The behavior of temperature profiles of fluid for $y = 0.1, 0.3, 0.5, 0.7, 0.9$ and $\mathrm{Pr} = 0.04, 0.733$ and 6.75 have been illustrated in Figs. 10-12, respectively. These figures are depicting a comparison of the heat transfer from the wall CD towards the wall AB of the rectangular physical domain considered. It has been concluded from Figs. 10-12 that the heat transfer for fluids like mercury, air and water has been found to be increasing towards the left side of the rectangular domain.

TABLE 3. Numerical solutions of pressure for Re = 1000.

(x,y)	p-pressure
$(0.3,0,1)$	0.00129
$(0.3,0.3)$	0.00470
$(0.3,0.5)$	0.00646
$(0.3,0.7)$	0.00706
$(0.3,0.9)$	0.01709
$(0.9,0.1)$	0.00101
$(0.9,0.3)$	0.00484
$(0.9,0.5)$	0.00722
$(0.9,0.7)$	0.01092
$(0.9,0.9)$	0.01035
$(1.5,0.1)$	0.00149
$(1.5,0.3)$	0.00423
$(1.5,0.5)$	0.00780
$(1.5,0.7)$	0.01022
$(1.5,0.9)$	0.01241
$(2.1,0.1)$	0.00393
$(2.1,0.3)$	0.00757
$(2.1,0.5)$	0.00797
$(2.1,0.7)$	0.01052
$(2.1,0.9)$	0.01464
$(2.7,0.1)$	0.00143
$(2.7,0.3)$	0.00491
$(2.7,0.5)$	0.00811
$(2.7,0.7)$	0.01173
$(2.7,0.9)$	0.01629

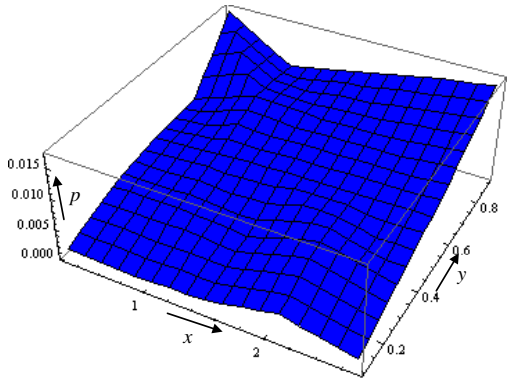

FIGURE 9. Pressure for (Re = 1000).

TABLE 4. Numerical solutions of temperature for different fluids.

(x,y)	T(Pr=0.04)	T(Pr=0.733)	T(Pr=6.75)
$(0.3,0,1)$	0.76584	0.72158	0.61471
$(0.3,0.3)$	0.81983	0.84563	0.67950
$(0.3,0.5)$	0.82267	0.86715	0.65997
$(0.3,0.7)$	0.81695	0.84523	0.67951
$(0.3,0.9)$	0.76798	0.72270	0.60622
$(0.9,0.1)$	0.71496	0.68370	0.74924
$(0.9,0.3)$	0.75694	0.81237	0.76912
$(0.9,0.5)$	0.75776	0.83674	0.75106
$(0.9,0.7)$	0.75687	0.81126	0.81721
$(0.9,0.9)$	0.71479	0.68313	0.84931
$(1.5,0.1)$	0.76584	0.72145	0.81471
$(1.5,0.3)$	0.81987	0.84568	0.87950
$(1.5,0.5)$	0.82268	0.86725	0.85997
$(1.5,0.7)$	0.81976	0.84515	0.87951
$(1.5,0.9)$	0.76569	0.72164	0.89622
$(2.1,0.1)$	0.87496	0.72158	0.86912
$(2.1,0.3)$	0.79168	0.84563	0.87499
$(2.1,0.5)$	0.78912	0.86735	0.90172
$(2.1,0.7)$	0.79194	0.84573	0.92496
$(2.1,0.9)$	0.79867	0.86745	0.91529
$(2.7,0.1)$	0.83311	0.85271	0.92106
$(2.7,0.3)$	0.91096	0.93770	0.94721
$(2.7,0.5)$	0.93387	0.94886	0.96529
$(2.7,0.7)$	0.90078	0.93846	0.95106
$(2.7,0.9)$	0.92274	0.95533	0.98418

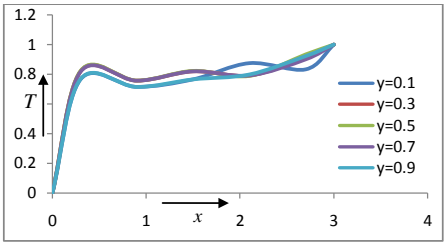

FIGURE 10. Temperature profiles for $(\mathrm{Pr} = 0.04)$.

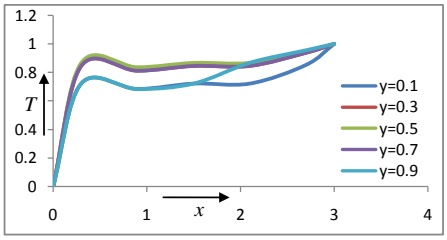

FIGURE 11. Temperature profiles for $(\mathrm{Pr} = 0.733)$.

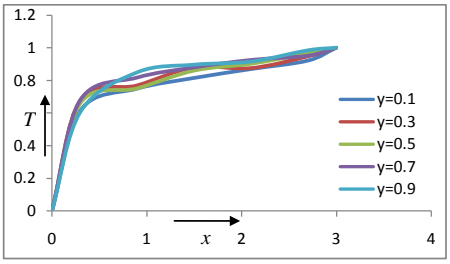

FIGURE 12. Temperature profiles for $(\mathrm{Pr} = 6.75)$.

TABLE 5. Numerical solutions of concentration for different fluids.

(x,y)	$C(\mathrm{Sc}=0.22)$	$C(\mathrm{Sc}=0.60)$	$C(\mathrm{Sc}=0.75)$
$(0.3,0.1)$	0.74684	0.72143	0.61323
$(0.3,0.3)$	0.82688	0.84662	0.66785
$(0.3,0.5)$	0.82145	0.85761	0.64567
$(0.3,0.7)$	0.81645	0.83512	0.66879
$(0.3,0.9)$	0.75678	0.71270	0.61522
$(0.9,0.1)$	0.70396	0.67370	0.73469
$(0.9,0.3)$	0.73467	0.80247	0.75812
$(0.9,0.5)$	0.74976	0.82346	0.73416
$(0.9,0.7)$	0.72346	0.82341	0.81672
$(0.9,0.9)$	0.71349	0.67313	0.83931
$(1.5,0.1)$	0.75684	0.73445	0.82471
$(1.5,0.3)$	0.81987	0.83568	0.86950
$(1.5,0.5)$	0.83468	0.85625	0.84397
$(1.5,0.7)$	0.80976	0.82515	0.78951
$(1.5,0.9)$	0.75569	0.71164	0.88622
$(2.1,0.1)$	0.87496	0.72158	0.86912
$(2.1,0.3)$	0.78168	0.83563	0.86499
$(2.1,0.5)$	0.78691	0.84735	0.92172
$(2.1,0.7)$	0.81194	0.86573	0.95496
$(2.1,0.9)$	0.79867	0.83745	0.90529
$(2.7,0.1)$	0.81111	0.84271	0.91106
$(2.7,0.3)$	0.90096	0.92370	0.93721
$(2.7,0.5)$	0.93387	0.94886	0.96529
$(2.7,0.7)$	0.90078	0.93846	0.95106
$(2.7,0.9)$	0.91274	0.93533	0.94180

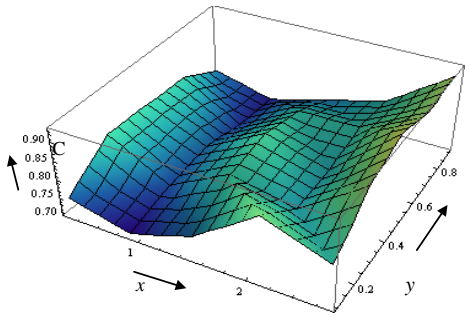

FIGURE 13. Concentration profiles for hydrogen $(\mathrm{Sc} = 0.22)$.

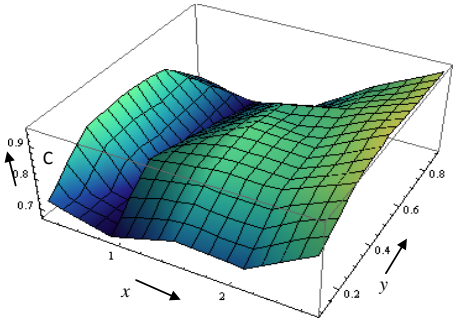

FIGURE 14. Concentration profiles for water vapour $(\mathrm{Sc} = 0.60)$.

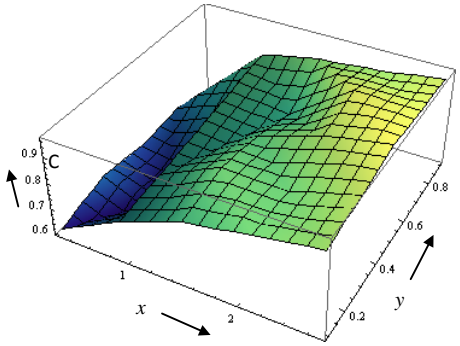

FIGURE 15. Concentration profile for oxygen $(\mathrm{Sc} = 0.75)$.

The numerical solutions of concentration profiles of flow for different Schmidt numbers $\mathrm{Sc} = 0.22, 0.60$ and 0.75 have been shown in Table 5. It has been depicted from Table 5 that concentration profiles of the fluid at particular value of y increases along x-axis. The behavior of concentration profiles for different fluids such as hydrogen $(\mathrm{Sc} = 0.22)$, watervapour $(\mathrm{Sc} = 0.60)$ and oxygen $(\mathrm{Sc} = 0.75)$ when grid node along x-direction is kept fixed at 0.3 to 2.7

while gird node along y-direction varied between 0.1, 0.3, 0.5, 0.7, 0.9 has been examined and illustrated in Figs. 13-18. The variation of the concentration considered in z-direction vis-á-vis grid nodes in x and y-direction has been examined and plotted using 3-D graphs and is given in Figs. 13-15. These figures are depicting a comparison of the mass transfer from the wall CD towards the wall AB of the rectangular physical domain considered. The variation of the concentration vis-á-vis grid nodes in x and y-direction has been examined and plotted using 2-D graphs and is given in Figs. 16-18. It has been observed from Figs. 13-18 that the mass transfer for fluids like hydrogen, water vapour and oxygen has been found to be increasing towards the left side of the rectangular domain. In case of hydrogen $(\mathrm{Sc} = 0.22)$, the mass transfer has been found to increase slightly and then decreases gradually. In case of water vapour $(\mathrm{Sc} = 0.60)$, the mass transfer increases steadily and then decreases steadily. The mass transfer has been found to increase gradually and then decreases while moving from left to the right. In case of hydrogen $(\mathrm{Sc} = 0.22)$, the mass transfer has been found to increase slightly and then decreases gradually. In case of water vapour $(\mathrm{Sc} = 0.60)$, the mass transfer increases steadily and then decreases steadily. In case of oxygen $(\mathrm{Sc} = 0.75)$, the mass transfer has been found to increase steadily and then decreases while moving from left to the right. The mass transfer has been found to oscillate when x is fixed at 2.1 and 2.7, y varied from 0.1 to 0.9. The mass transfer has been found to increase steadily and then decreases while moving from left to the right. The mass transfer has been found to oscillate in all the cases of hydrogen $(\mathrm{Sc} = 0.22)$, water vapour $(\mathrm{Sc} = 0.60)$ and oxygen $(\mathrm{Sc} = 0.75)$ when x is fixed at 2.1, 2.7 and y varied from 0.1 to 0.9.

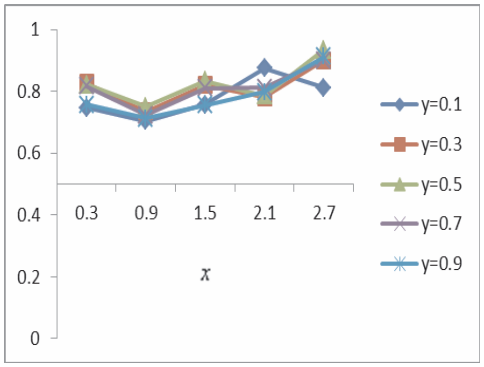

FIGURE 16. Concentration profile for hydrogen $(\mathrm{Sc} = 0.22)$.

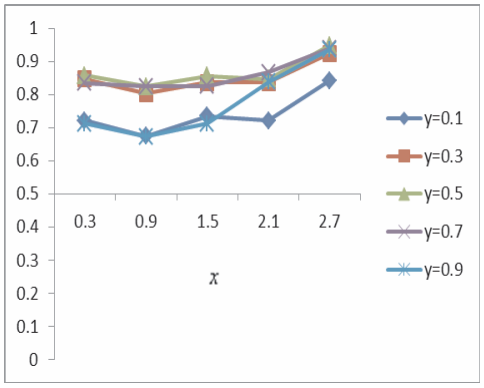

FIGURE 17. Concentration profile for water vapour (Sc = 0.60).

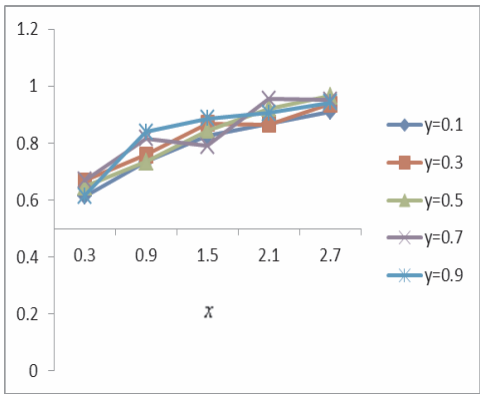

FIGURE 18. Concentration profile for oxygen (Sc = 0.75).

6. Conclusions

In this paper, coupled fluid flow with heat and mass transfer has been numerically investigated using a finite volume method. The numerical results for flow variables together with heat and mass transfer for different non-dimensional parameters like Reynolds number Re = 1000, Prandtl number Pr = 0.04, 0.733 and 6.75 and Schmidt numbers Sc = 0.22, 0.60, and 0.75 have been obtained. These values are kept fixed at Pr = 0.04, 0.733, 6.75 and Sc = 0.22, 0.60, 0.75 which corresponds to mercury, air, water and hydrogen, watervapour, oxygen respectively by considering its physical significance into account as input data while performing numerical computations.

The behaviour of u-velocity and v-velocity for Reynolds number $\mathrm{Re} = 1000$ at different nodes has been examined using 3-D graphs. It has been observed that for fixed value of y, u-velocity decreases initially and then keeps on increasing uniformly as we move from left boundary to the right boundary and for fixed value of x, v-velocity increases at external nodes and has an oscillatory behavior at internal nodes as we move from bottom boundary to top boundary of the physical domain.

The behaviour of pressure and the variation of the concentration considered in z-direction vis-á-vis grid nodes in x and y-direction has been plotted and examined using 3-D graphs. It has also been observed that either keeping x-fixed or y-varies or keeping y-fixed and the pressure increases uniformly. It has been observed that the heat transfer for fluids like mercury, air and water has been found to be increasing towards the left side of the rectangular domain. The mass transfer has been found to increase steadily and then decreases while moving from left to the right. In case of watervapour $(\mathrm{Sc} = 0.60)$, the mass transfer increases steadily and then decreases steadily. In case of oxygen $(\mathrm{Sc} = 0.75)$, the mass transfer has been found to increase steadily and then decreases while moving from left to the right. The mass transfer has been found to oscillate in all the cases of hydrogen $(\mathrm{Sc} = 0.22)$, watervapour $(Sc = 0.60)$ and oxygen $(\mathrm{Sc} = 0.75)$ when x is fixed at 2.1, 2.7 and y varied from 0.1 to 0.9.

Nomenclature

p	thermodynamic pressure
P	dimensionless pressure
Re	Reynolds number
Pr	Prandtl number
Sc	Schmidt number
C	concentration
T	temperature
u	velocity vector
x, y	co-ordinates
t	dimensionless time
Δx	grid spacing along x-axis

Δy grid spacing along y-axis

u x-component of the velocity

v y-component of the velocity

u^* initial guess for x-component of the velocity

v^* initial guess for y-component of the velocity

p^* initial guess for pressure

T^* initial guess for temperature

c^* initial guess for concentration

p' pressure correction

F_w convective flux per unit mass at west face

F_e convective flux per unit mass at east face

F_s convective flux per unit mass at south face

F_n convective flux per unit mass at north face

D_w diffusivity conductance at west face

D_e diffusivity conductance at east face

D_s diffusivity conductance at south face

D_n diffusivity conductance at north face

Greek symbol

ρ density

Subscripts

i Index used in tensor notation

j Index used in tensor notation

e, w, n, s east, west, north, south faces

Conflict of Interests

The authors declare that there is no conflict of interests.

Acknowledgements

The author acknowledge the support from the University of Delhi under R&D and doctoral research programme for providing research grant vide letter no. DRCH/R&D/2013-14/4155 dated 21 October 2013 to carry out this work.

REFERENCES

[1] F.H. Harlow and J.E. Welch, Numerical calculations of time-dependent viscous incompressible flow of fluid with free surface, Phys. Fluids, 8 (12) (1965) 2182–2189.

[2] L.E. Erickson, L.T. Fan and V.G. Fox, Heat and mass transfer on moving continuous flat plate with suction or injection, Ind. Eng. Chem. Fundam., 5 (1966) 19–25.

[3] A.J. Chorin, Numerical solution of the Navier-Stokes equations, Math. Compt., 22 (1968) 745–762.

[4] S.V. Patankar and D.B. Spalding, A calculation procedure for heat, mass and momentum transfer in three-dimensional parabolic flows, Int. J. Heat Mass Transfer, 15 (1972) 1787–1806.

[5] P.S. Gupta and A.S. Gupta, Heat and mass transfer on a stretching sheet with suction or blowing, Can. J. Chem. Eng., 55 (1977) 744–746.

[6] Suhas V. Patankar, Numerical Heat Transfer and Fluid Flow, Hemisphere, New York, 1980.

[7] U. Ghia, K.N. Ghia and C.T. Shin, High-resolutions for incompressible flow using the Navier-Stokes equations and a multigrid method, J. Comput. Phys., 48 (1982) 387–411.

[8] R. Schreiber and H.B. Keller, Driven cavity flow by efficient numerical techniques, J. Comput. Phys., 49 (1983) 310–333.

[9] R. Peyret and T.D. Taylor, Computational Methods for Fluid Flow, Springer-Verlag, New York (1983).

[10] N. Chen, H.W. Ryu, D.H. Park and Y.S. Park, Effect of external laminar channel flow on mass transfer in a cavity, Int. J. Heat Mass Transfer, 30 (1987) 2137–2149.

[11] K.N. Lakshmisha, S. Venkateswaran and G. Nath, Three-dimensional unsteady flow with heat and mass transfer over a continuous stretching surface, J. Heat Transfer, 110 (1988) 590–595.

[12] K.N. Ghia and U. Ghia, Elliptic systems: finite-difference method III, Handbook of Numerical Heat Transfer, eds. W.J. Minkowycz et al., Wiley, 1988.

[13] M.L. Mansour and A. Hamed, Implicit solution of the incompressible Navier-stokes equations on non-staggered grid, J. Comput. Phys., 86 (1990) 147–167.

[14] C.H. Bruneau and C. Jouron, An efficient scheme for solving steady incompressible Navier-Stokes equations, J. Comput. Phys., 89 (1990) 389–413.

[15] C. Alkire, H. Deligianni and J.B. Ju, Effect of fluid flow on convective transport in small cavities, J. Electrochem. Sco., 137 (1990) 818–824.

[16] I. Demirdzic and M. Peric, Finite volume methods for prediction of fluid flow in arbitrarily shaped domains with moving boundaries, Int. J. Num. Meth. Fluids, 10 (1990), 771–790.

[17] P. Le Quere, Accurate solution to the square thermally driven cavity at high Rayleigh number, Computer Fluids, 20 (1991) 29–41.

[18] M. Occhialini and J.J.L. Higdon, Convective mass transport from rectangular cavities in viscous flow, J. Electrochem. Soc., 139 (1992) 2845–2855.

[19] Z. Lilek and M. Peric, A fourth-order finite volume method with collocated variable arrangement, Computers and Fluids, 24 (1995) 239–252.

[20] J.D. Anderson, Computational Fluid Dynamics with Basics and Applications, McGraw-Hill, New York, 1995.

[21] H. Chen, Effect of the aspect ratio on the transient mass/heat transfer in an open cavity, J. Chinese Inst. Engrs. 19 (1996) 273.

[22] D.A. Anderson, R.H. Pletcher and J.C. Tanneihill, Computational Fluid Mechanics and Heat Transfer, 2nd ed., Taylor and Francis, Washington D.C., 1997.

[23] Y.A. Shehata, V. Modi and A.C. West, Mass transfer to a channel wall downstream of a cylinder, Int. J. Heat Mass Transfer, 40 (1997) 4263–4271.

[24] A. Postelnicu, Influence of a magnetic field on heat and mass transfer by natural convection from vertical surface in porous media considering Soret and Dufur effects, Int. J. Heat Mass Transfer, 47 (2004) 1467–1472.

[25] S.A. Salem, On the numerical solution of the incompressible Navier-Stokes Equations in primitive variables using grid generation techniques, Mathematical and Computational Applications, 11 (2006) 127–136.

[26] C.H. Bruneau and M. Saad, The 2-D lid-driven cavity problem revisited, Computers and Fluids, 35 (2006) 326-348.

[27] D.L. Young, S.J. Jane, C.M. Fan, K. Murugesan and C.C. Tsai, The method of fundamental solutions for 2-D and 3-D Stokes problems, J. Comput. Phys., 211 (2006) 1–8.

[28] M. Tirumaleshwar, Fundamentals of Heat and Mass Transfer, First impression, Pearson, India (2006).

[29] H.K. Versteeg and W. Malalsekra, An Introduction to Computational Fluid Dynamics: The Finite Volume Method, 2nd ed., Pearson, India (2007).

[30] A. Hokpunna and M. Manhart, Compact fourth-order finite volume method for numerical solutions of Navier-Stokes equations on staggered grids, J. Comput. Phys., 229 (2010) 7545–7470.

[31] S. Biringen and C.Y. Chow, An Introduction to Computational Fluid Mechanics by Example, John Wiley & Sons, New Jersey (2011).

[32] A.K. Shehata, J.D. Yang, A.C. West, P.V. Modi, Effect of an unsteady external flow on mass transfer to cavities, Int. J. Heat Mass Transfer, 42 (1999) 673–683.